Lab on a Chip

RSC Publishing

PAPER

View Article Online
View Journal | View Issue

Electrochemical detection of individual DNA hybridization events†

Cite this: *Lab Chip*, 2013, **13**, 349

Timothy M. Alligrant, Elizabeth G. Nettleton and Richard M. Crooks*

Received 30th August 2012,
Accepted 8th November 2012

DOI: 10.1039/c2lc40993c

www.rsc.org/loc

We report on real-time electrochemical detection of individual DNA hybridization events at an electrode surface. The experiment is carried out in a microelectrochemical device configured with a working electrode modified with single-stranded DNA probe molecules. When a complementary DNA strand labelled with a catalyst hybridizes to the probe, an easily detectable electrocatalytic current is observed. In the experiments reported here, the catalyst is a platinum nanoparticle and the current arises from electrocatalytic oxidation of hydrazine. Two types of current transients are observed: short bursts and longer-lived steps. At low concentrations of hydrazine, the average size of the current transients is proportional to the amount of hydrazine present, but at higher concentrations the hydrazine oxidation reaction interferes with hybridization.

Introduction

In this paper, we describe an electrochemical method for real-time detection of single-oligonucleotide hybridization events. The approach is outlined in Fig. 1. Briefly, a Au microband electrode is photolithographically defined, modified with single-stranded DNA (ssDNA) probes (green strand, Fig. 1), and then affixed to a poly(dimethylsiloxane) (PDMS) monolith containing a single microchannel. Next, a flowing aqueous solution containing hydrazine (N_2H_4) is introduced at the inlet of the fluidic channel and a background current *versus* time (*i*–*t*) transient is obtained (represented by the red *i*–*t* curve and red reaction in Fig. 1). In this case, the current is minimal, because N_2H_4 is electroinactive at the Au electrode at the potential at which the measurement is performed. Finally, a solution containing both N_2H_4 and 4 nm Pt nanoparticles conjugated to complementary DNA targets (PtNP-cDNA) is introduced, and then the same *i*–*t* experiment is carried out. In this case, an increase in anodic current is observed (blue curve and blue reaction, Fig. 1), corresponding to hybridization of a single DNA target and subsequent electrocatalytic oxidation of N_2H_4 at the PtNP (eqn (1)). This finding is significant, because it provides a basis for studying single hybridization events in real-time using electrochemical methods and designing highly sensitive chemical sensors.

$$N_2H_4 = N_2 + 4H^+ + 4e^- \quad (1)$$

The results reported here are based on earlier reports related to PtNP tagging of DNA and electrocatalytic amplification (ECA) arising from hybridization.[1] For example, Mirkin and coworkers previously described a DNA sandwich array based on DNA probes bound to a glass surface and detection strands conjugated to Au nanoparticles.[2,3] Utilizing a signal amplification method involving Ag electroless deposition and a flatbed scanner, they determined the presence of a DNA target at a limit of detection (LOD) of 50 fM. When the detection modality was surface enhanced Raman scattering spectroscopy the unoptimized detection limit was 20 fM. Willner and coworkers reported a method for direct faradic electrochemical detection of DNA based on the electrocatalytic oxidation of H_2O_2 initiated by hybridization of PtNP-tagged DNA.[4] They also reported a related approach based on chemiluminescence detection,[5] and in both cases the LOD for DNA detection was 10 pM. We subsequently adopted these

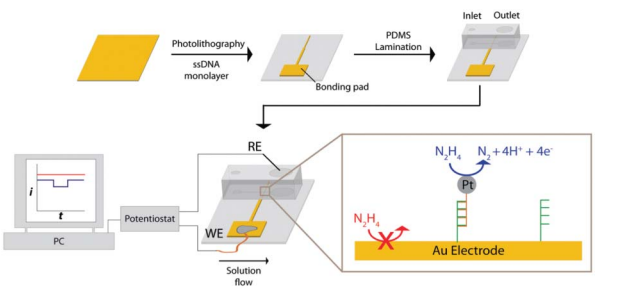

Fig. 1 Device fabrication and implementation for electrocatalytic amplification in a microfluidic device.

Department of Chemistry and Biochemistry, Center for Electrochemistry, and Center for Nano- and Molecular Science and Technology, The University of Texas at Austin, Austin, TX 78712-0165, USA. E-mail: crooks@cm.utexas.edu

† Electronic supplementary information (ESI) available: Includes additional experimental details including: characterization of PtNPs, preparation of PtNP-DNA conjugates, a figure depicting device fabrication, supplementary electrochemical data and controls, additional experimental details and XPS data. See DOI: 10.1039/c2lc40993c

types of methods to signal DNA hybridization on bipolar electrodes.[6,7] Kwon and Bard used an experimental method similar to that of Willner, and they were also able to detect DNA hybridization at target concentrations as low as 10 pM.[8] However, in some cases their experiments were sufficiently sensitive that they also detected the signature of individual electrocatalytic events after equilibrating a DNA-modified electrode for 30 min with a 10 μM solution of reporter strands bearing PtNP labels. Presumably this observation was a consequence of only a small number of surface-bound labels having access to the electrode

Another important precedent for our study is recent real-time electrochemical single-particle detection described by Bard and coworkers.[9–11] These experiments are set up by poising the potential of a working electrode at a value at which little faradic current flows, even in the presence of a high concentration of a kinetically slow redox molecule. Now, when NPs, which are catalytic for oxidation or reduction of the redox molecule, are added to the solution, individual current transients are observed. These transients represent collisions between individual NPs and the electrode surface. A number of different types of NPs (Pt, Au, and IrO_x), working electrodes (Au, Pt, Pt-PtO_x, and carbon), and redox molecules (N_2H_4, water (OH^-), H_2O_2, H^+, and BH_4^-) exhibit this behavior and demonstrate the generality of the ECA method.[9] The Compton group has also made major contributions to the field of ECA.[1,12–18] Their primary focus has been on deriving fundamental information about collisions by studying electrodeposition[16,18] and electrodissolution[12,13] of individual NPs. However, they have also carried out studies involving NPs tagged with electroactive groups.[14]

The focus of the present manuscript is real-time electrochemical detection of DNA hybridization. However, other (non-electrochemical) methods have been reported that also achieve this goal. For example, a nanoscale field-effect transducer (FET) device was used to detect unlabeled single-oligonucleotide hybridization in real-time, and to evaluate binding kinetics and thermodynamics.[19] Another example of single-oligonucleotide hybridization utilizes an optical method.[20] Here, a silica microparticle-labeled DNA probe is bound to a glass surface and the displacement of a microparticle is monitored *via* evanescent wave scattering. Our electrochemical approach is quite a bit simpler than these other methods and better suited to biosensing applications.

In the present study, a Au microband electrode was modified with ssDNA sequences, and the real-time hybridization of individual PtNP-cDNA, present at concentrations as low as 25 pM, was observed as current steps arising from the electrocatalytic oxidation of N_2H_4. Importantly, identical experiments carried out using PtNP-labelled non-complementary DNA (PtNP-ncDNA) do not exhibit current transients. Moreover, experiments carried out using PtNP-cDNA conjugates on ssDNA-free (naked) Au electrodes do not exhibit current steps, indicating that nonspecific adsorption (NSA) is not a significant barrier to implementing this approach for chemical sensing applications. This result is similar to the E-DNA biosensing approach of Plaxco and coworkers, which have also exhibited little influence of NSA.[21,22]

Experimental

Chemicals

The following chemicals were purchased from Sigma-Aldrich (St. Louis, MO) and used as received: hydrazine monohydrate (64% N_2H_4, 98%), tris(2-carboxyethyl)phosphine hydrochloride (TCEP, 98.0%), tris(hydroxymethyl)aminomethane hydrochloride (tris-HCl, 99.8%), chloroplatinic acid (H_2PtCl_6, 99.995%), sodium borohydride ($NaBH_4$, 99.0%), PerfectHyb Plus Hybridization buffer (hybridization buffer, 1×), and iodine (99.8%). The following chemicals were purchased from Fisher Scientific (Fair Lawn, NJ) and used as received: sodium dihydrogen phosphate dihydrate (100%), hydrochloric acid (HCl, 37% in water), acetone (99.9%), sodium chloride (100%), disodium ethylenediamine tetraacetic acid (EDTA, 99.0%). The following additional chemicals were used as received: sodium citrate (EM Science, Gibbstown, NJ), sodium hydroxide (NaOH, 97.0%, EMD Chemical) and potassium iodide (KI, 100%, Mallinckrodt). Deionized water from a Millipore filtration system (Milli-Q gradient system, Millipore, Bedford, MA) having a resistivity of 18.2 MΩ cm was used for all experiments.

Preparation of oligonucleotide solutions

All DNA oligonucleotides were synthesized and purified (HPLC) by Integrated DNA Technologies (IDT, Coralville, IA) and received as lyophilized pellets. The sequences of each of these oligonucleotides is listed in Table 1. Prior to use, the ssDNA, cDNA and ncDNA strands were each rehydrated in a pH 7.4, 0.10 M phosphate buffered, 10.0 mM TCEP solution for 1 h at 24–25 °C to cleave the disulfide bond used to stabilize the thiol modification during shipping. A 100.0 μL aliquot of this solution was then placed in a G-25 Sephadex microcentrifuge column (GE Healthcare, Piscataway, NJ) to remove TCEP and mercaptopropanol produced by the disulfide reduction. This separation was carried out according to the protocol provided by the manufacturer. Finally, a 100.0 μL aliquot of 20.0 mM tris-HCl, 2.0 mM EDTA, and 0.20 M NaCl (pH 7.4, 2× TE buffer) solution was added to the filtered DNA solution. This addition yielded a final TE buffer concentration of 10.0 mM tris-HCl, 1.0 mM EDTA and 0.10 M NaCl, pH 7.4 (1× TE buffer). The stock solutions of DNA in TE buffer were stored at −20 °C until ready for use.

Synthesis of platinum nanoparticles

The synthesis of the PtNPs followed a previously described method.[6] Briefly, 15.0 mL of a 500.0 μM H_2PtCl_6 solution was mixed with 1.0 mL of a 50.0 mM sodium citrate solution in a glass vial. Next, 500 μL of a 30.0 mM $NaBH_4$ solution was added drop-wise with a pipette in 5.0 μL additions, while stirring at 24–25 °C. The vial was sealed and stirred for an additional 30 min. Next, the entire solution was transferred to a 35 mm dialysis sack (12 000 Da MWCO, Sigma-Aldrich) and placed in a 4 L beaker filled with deionized water for 24 h to

Table 1 DNA sequences utilized in this study

Sequence name	Sequence
Probe (ssDNA)	5′-CAC GAC GTT GTA AAA CGA CGG CCA G-$(CH_2)_3$ SH-3′
Target (cDNA)	5′-CTG GCC GTC GTT TTA CAA CGT CGT G-$(CH_2)_3$ SH-3′
Non-complementary target (ncDNA)[a]	5′-CTG GCC GTC **TCC CGA** CAA CGT CGT G-$(CH_2)_3$ SH-3′

[a] Non-complementary region shown in bold.

remove excess salts. Finally, the PtNPs were characterized by transmission electron microscopy (TEM, FEI Tecnai TEM). A representative TEM image and size distribution histogram are provided in the Electronic Supplementary Information (Fig. S1†).

Device fabrication

The Au microband electrodes were prepared on 25 × 38 mm glass slides using standard photolithographic methods, which we have described previously.[6] A positive photoresist layer (~10 μm thick, AZ P4620, AZ Electronic Materials, Branchburg, NJ) was spin-coated onto Au-coated glass (100 nm Au layer, EMF Corp., Ithaca, NY) using a three-step spin program, and then exposed to UV light through a positive photomask (CAD/Art Services, Inc., Bandon, OR). The photomask, and ultimately the device pattern, consisted of a 25 μm × 7 mm microband and a 3 × 5 mm rectangular contact pad. After removal of the UV-exposed photoresist using a developer solution (AZ 421 K, AZ Electronic Materials, Branchburg, NJ), the unprotected Au was removed using an aqueous solution of 5% I_2 and 10% KI (for ~2 min). Next, the remaining photoresist was removed with acetone. Finally, contact to a potentiostat was made to the patterned slide with a ~15 mm-long copper wire (24 AWG, Fisher Scientific), attached to the Au contact pad with silver epoxy (Electron Microscopy Sciences, Hatfield, PA) and insulated with 5-minute epoxy (Grainger, Inc., Lake Forest, IL). Fig. S2a† is a photograph of the device at this point in the fabrication process.

Following development of the slide, the gold microband was modified with ssDNA using a procedure similar to that previously described.[6] First, a 30.0 μL aliquot of 1.0 μM TCEP-digested ssDNA solution was prepared in 1× TE buffer and placed directly on the microband electrode for 2 h in a humidity chamber (20–25 °C, 85–90% humidity). Then, the microband was washed with deionized water for 20 s and dried with a stream of N_2. The ssDNA surface density, measured using a standard electrochemical method[23] and four independently prepared electrodes, was $(1.8 \pm 1.0) \times 10^{13}$ molecules cm^{-2}.

The microfluidic channel was prepared *via* soft lithography using poly(dimethylsiloxane) (PDMS, Slygard 184, Dow Corning, Midland MI) and a literature micromolding technique.[24] The dimensions of the channel were 6 mm long, 25 μm wide, and 20 μm high. Two reservoirs were punched at either end of the channel using Harris Uni-Core coring punches (Ted Pella, Redding, CA). A 0.75 mm-diameter reservoir served as the fluidic inlet and a 4.0 mm-diameter reservoir served as the outlet. The PDMS monolith was then exposed to an air plasma (60 W, model PDC-32G, Harrick Scientific, Ossining, NY) for 45 s. Then, the microchannel-containing-PDMS monolith was joined to the ssDNA-modified, Au microband supported glass slide. The PDMS was oriented so that the microchannel was aligned perpendicular to the microband (Fig. S2b†) and so that the reservoir used to host the reference electrode was positioned only 200–500 μm away from the working electrode to minimize the ohmic potential drop within the channel.[25] Next, a 1.5 mm-thick polystyrene plate with an oblong hole cut into it was placed over the PDMS and three binder clips were used to secure it in place as shown in Fig. S2c†. This clamping arrangement, along with large PDMS monoliths (~25 × ~25 mm), ensured that the microchannel did not leak. Finally, the hybrid PDMS/glass microfluidic device was connected to a 50.0 μL syringe (Hamilton, Reno, NV) secured in a syringe pump (Pump 11, Pico Plus Elite, Harvard Apparatus, Holliston, MA) using Teflon tubing (Cole-Parmer, Vernon Hills, IL).

Pt microband electrodes were prepared *via* a lift-off photolithographic method. LOR 10B (Microchem, Newton, MA) was spin-coated onto silicon wafers having a 1 μm-thick silicon dioxide layer (University Wafers, South Boston, MA). After baking for 5 min, an additional S 1811 photoresist (Shipley, Marlborough, MA) layer was deposited and baked for 1 min. The wafer was then exposed to UV light through a negative photomask, which patterned ~20 μm microband electrodes connected to rectangular contact pads. Next, the exposed surface was developed in a 1 : 4 dilution of AZ 400 K developer (AZ Electronic Materials, Branchburg, NJ) for ~1 min. Following photolithography, the wafers were sent to LGA Thin Films (Santa Clara, CA) for evaporation of a 5 nm Ti adhesion layer followed by 100 nm of Pt. Liftoff was performed for 20 min in 60 °C PG Remover (Microchem, Newton, MA). The slides were rinsed with ethanol, then deionized water. Electrical connections were established as described earlier.

The PDMS microchannel was attached to the Pt/silicon dioxide substrate in a manner similar to that described for the Au/glass devices. However, in this case, both the silicon substrate and the PDMS monolith were exposed to the oxygen plasma for 45 s before pressing the components together without the use of the binder clip arrangement described by Fig. S2c†. The completed device was heated on a 60 °C hotplate for 5 min before use.

Electrochemistry

Cyclic voltammetry (CV) and *i–t* curves obtained using Au microband devices were measured using a potentiostat and Faraday cage similar to that described by Zhang and coworkers.[26,27] A Chem-Clamp voltammeter-amperometer (Dagan Corp., Minneapolis, MN) served as the potentiostat, while the voltage signal was generated by a PAR 175 (Princeton Applied Research, Oak Ridge, TN) universal function generator. This setup was interfaced to a Dell Optiplex 380 computer through a PCI-6251 data acquisition board (National Instruments, Austin, TX) *via* a BNC-2090A analog breakout accessory (National Instruments, Austin, TX). Two-electrode cell connections from a preamplifier were housed in a Faraday cage constructed of copper plate and mesh. The voltammetric data

and *i–t* curves were measured using custom software written in LabView 2010 (National Instruments, Austin, TX). The sampling rate for measuring both CVs and *i–t* curves with this instrument was 100 measurements s^{-1}.

CV measurements using the Pt microband devices, as well as the Pt and Au ultramicroelectrodes (UMEs), were made using a CHI 650C potentiostat (Austin, TX). Additionally, AC voltammetry was measured using the same CHI potentiostat from −0.6 to 0.6 V *vs.* Ag/AgCl. The parameters for the AC voltammetric measurements were: a frequency of 1 Hz, a step potential of 20 mV, and amplitude of 3 mV. AC voltammograms were obtained by placing the Au-patterned microband devices directly in a 50.0 mM phosphate buffer solution (pH 7.0), both before and after ssDNA modification. Attempts were made to record lower frequency AC voltammograms (0.2 to 0.5 Hz), however, these voltammograms typically exhibited significant noise due to the non-ideal electrode geometry (~10–15 mm long microband). All potentials reported herein were referenced to a "leakless" Ag/AgCl reference electrode (3.4 M KCl, model 66-EE009, Dionex, Bannockburn, IL).

Results and discussion

Fig. 2a shows cyclic voltammograms (CVs) obtained at a ssDNA-modified Au electrode in the absence (black) and presence (red) of N_2H_4 using the microelectrochemical device illustrated in Fig. 1. The featureless black CV was obtained first, and it is characteristic for the conditions used in our experiments (aqueous 50 mM phosphate buffer, pH 7, flow rate = 50.0 nL min^{-1}).[28,29] Next, the same buffer solution, but now containing 5.0 mM N_2H_4, was introduced into the microchannel at the same flow rate (red CV). Consistent with prior reports, the onset of N_2H_4 oxidation is ~0.15 V *vs.* Ag/AgCl.[8,29]

After obtaining the CVs shown in Fig. 2a, a series of solutions, all containing phosphate buffer and 5.0 mM N_2H_4, were sequentially introduced into the fluidic channel, and the *i–t* data shown in Fig. 2b were obtained. Note that all of the data shown in Fig. 2 were collected using the same microelectrochemical device. The *i–t* data presented in Fig. 2b were measured by stepping the electrode potential from −0.20 V to 0.15 V (at the foot of the rising current transient shown in red in Fig. 2a). The value of the initial potential (−0.20 V) is important for three reasons: (1) it is sufficiently negative of the point of zero charge (pzc, 0.2–0.3 V) to inhibit hybridization of DNA prior to the beginning of the experiment; (2) it is not so negative as to greatly affect the conformation of the surface-confined ssDNA;[30–32] (3) it is in a potential region in which N_2H_4 oxidation does not proceed on a Au electrode. The final potential (0.15 V) is also important, because at this value N_2H_4 oxidation is facile on the PtNP labels but very slow on the Au electrode. This point is illustrated in Fig. S3†, where CVs collected on naked Au and Pt microelectrodes are presented alongside CVs obtained at a Au electrode functionalized with hybridized PtNP-labelled double-stranded DNA (PtNP-dsDNA). On the naked Pt electrode, the onset of N_2H_4 oxidation is

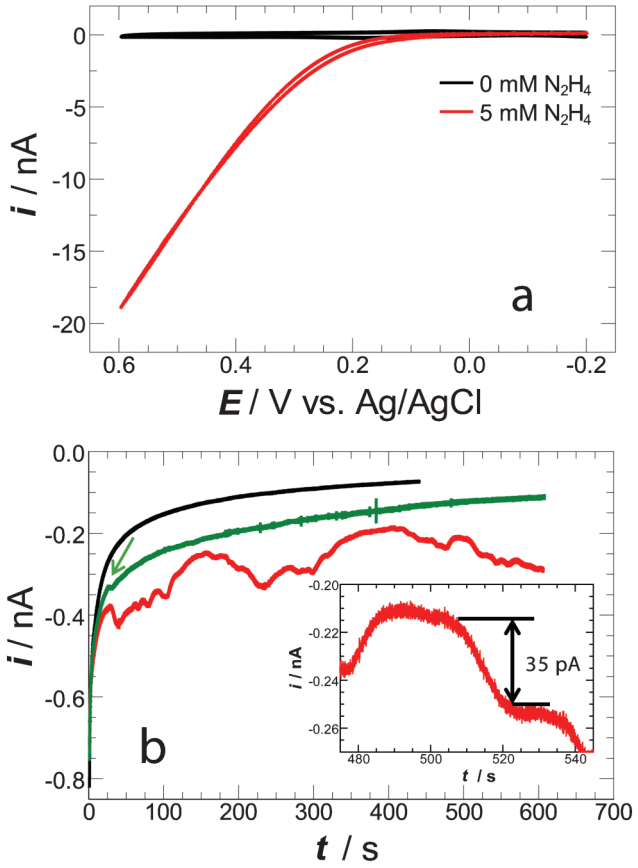

Fig. 2 Electrochemical measurements obtained using the microelectrochemical device illustrated in Fig. 1. (a) CVs obtained in the presence (red) and absence (black) of N_2H_4 at a ssDNA-modified 25 μm × 25 μm Au working electrode. Scan rate = 20 mV s^{-1}. (b) *i–t* curves measured at 0.15 V *vs.* Ag/AgCl. The Au electrode surface was modified with ssDNA (Table 1), and in addition to 5.0 mM N_2H_4, the solution contained (black) no target DNA, (green) 25 pM PtNP-ncDNA, and (red) 25 pM PtNP-cDNA. The inset shows an expanded region of the red *i–t* curve. Conditions: 50.0 mM phosphate buffer, pH 7.0, flow rate = 50 nL min^{-1}.

~0.3–0.5 V more negative relative to naked Au. On the PtNP-dsDNA-modified Au electrode the onset for N_2H_4 oxidation is shifted ~0.1 V negative relative to the ssDNA-modified electrode (Fig. S3d†).

The black trace in Fig. 2b represents a control experiment carried out using an electrode modified with ssDNA, but in the absence of solution-phase DNA (buffer + 5.0 mM N_2H_4 only). The only notable feature is the sharply rising current at $t = 0$, which may represent the initial nonfaradic charging of the electrochemical double layer associated with stepping the potential of the electrode from −0.20 V to 0.15 V.[25] Following this experiment, the solution in the microchannel was switched to one containing buffer, 5.0 mM N_2H_4, and, now, 25 pM PtNP-ncDNA. After stabilization of flow (~15 min, see ESI), the green trace was obtained. Compared to the black trace, this one displays more noise (we don't know why), but is otherwise comparable.

At this point in the experiment, a solution identical to that used to obtain the green trace, except now containing 25 pM

PtNP-cDNA, was introduced into the microchannel and the red trace was recorded. The differences between this result and the two control experiments are striking. Specifically, the red *i–t* data reveal several sharp increases in anodic current that persist for up to 100 s, after which the current typically regains its background value. As will be discussed shortly, results of this type were obtained in every one of the 15 experiments we carried out.

The increase in anodic current is due to hybridization of the PtNP-cDNA conjugates with the ssDNA bound to the Au electrode. Two types of current transients are observed: some have a stepped appearance (inset, Fig. 2b) and some are much sharper (see data between ~50 to 125 s, and *i–t* curves in Fig. S5†). The current transients in Fig. 2b range in magnitude from 11 to 43 pA and the average is 25 ± 10 pA. These values can be compared to values calculated using eqn (2), where n is the number of electrons transferred (4, eqn (1)), F is the Faraday constant, D is the diffusion coefficient of N_2H_4 (9.1×10^{-6} cm^2 s^{-1}), C is the concentration of N_2H_4 (5.0 mM), and r is the radius of the PtNPs.[33] The average value of r is 2.0 ± 0.4 nm and its range is 1.4 to 3.0 nm (Fig. S1b†). Using these values, the anticipated average current transient should be 31 pA and (on the basis of the particle-size distribution) the transients should span the range from 21 to 45 pA, which is in good agreement with the experimental observations. We performed multiphysics simulations of 1.0 to 4.0 nm-diameter spherical electrodes to ensure the validity of eqn (2) in the presence and absence of convection (50 nL min^{-1}). The simulated current values under convection deviated by no more than 0.02% from those determined in the absence of convection, and neither value deviated by more than 1.0% from eqn (2).

$$i = 4\pi(\ln 2)nFDCr \quad (2)$$

There were a few exceptions to the range and type of current transients discussed thus far. Specifically, ~4% of the transients had a magnitude in the range of 100–200 pA, which we believe arise from hybridization of PtNP-cDNA aggregates.[9,33] In addition, we occasionally observed small current transients in control experiments carried out using PtNP-ncDNA. In this case, between 1–3 transients were observed per 10 min observation window, and their magnitude was always <10 pA. One such transient (5 pA) is indicated by the green arrow in Fig. 2b.

In addition to the control experiments involving PtNP-ncDNA, controls involving the flow of naked PtNPs (no DNA) over ssDNA-modified electrodes and PtNP-cDNA conjugates over naked Au electrodes were performed. These experiments were used to assess NSA. Data for these additional controls can be found in the ESI. The *i–t* data obtained for both of these control experiments did not exhibit the characteristic current transients associated with NP-electrode collisions (Fig. S4†). This indicates that NSA is not an important factor in these experiments.

As shown by eqn (2), the current amplitude associated with a collision event should be proportional to the concentration of the substrate (N_2H_4 in this case). This proportionality has previously been shown to apply over a substrate concentration range of 10 mM to 15 mM for collisions of nominally naked nanoparticles at nominally naked electrodes.[33] Fig. 3 is a plot of average peak current *versus* the concentration of N_2H_4 obtained at a ssDNA-modified Au electrode in the presence of PtNP-cDNA. Representative *i–t* curves from which these data were extracted are provided in the ESI (Fig. S5†). At concentrations between 5.0 and 10.0 mM N_2H_4, the current transients increased from an average of 25 ± 10 to 67 ± 30 pA, respectively. However, at higher N_2H_4 concentrations, the currents actually decrease. This is likely due to local dehybridization of dsDNA arising from oxidation of N_2H_4 and the corresponding generation of H^+ (eqn (1)). This effect will be exacerbated at the highest N_2H_4 concentrations, particularly as the N_2H_4 concentration approaches that of the 50 mM phosphate buffer. Note that DNA dehybridization is known to occur at pH < 3 and pH > 10.[34] Moreover, electrogenerated pH changes to dehybridize surface-confined dsDNA has been previously proposed.[35,36]

Summary and conclusions

In conclusion, we have reported the first example of real-time single-oligonucleotide hybridization using electrochemical methods. The current amplification arising from electrocatalytic oxidation of a relatively high concentration of a sacrificial redox molecule, N_2H_4 in this case, enables these types of measurements. Although the results reported here are unambiguous and easily repeatable, they pose a number of interesting questions that require additional research. For

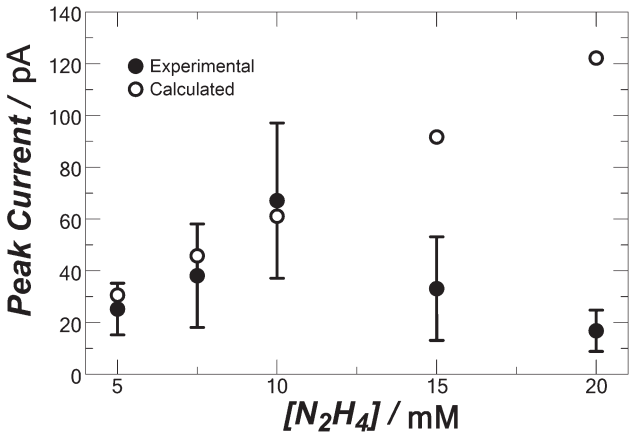

Fig. 3 Plot of the average magnitude of the current transient arising from electrocatalytic N_2H_4 oxidation as a function of the concentration of N_2H_4 in solution. The experimental conditions were the same as those used to acquire the data in Fig. 2, and in all cases the concentration of the labelled probe (PtNP-cDNA) was either 25 or 50 pM. The error bars represent the standard deviation of measured transients collected from at least three independent experiments.

example, we don't know the molecular-level origin of the sharp and stepped current transients shown in Fig. 2b. It is certainly possible that these current transients arise from a combination of new and old hybridization events. By this we mean that a hybridization event will give rise to a current transient upon initial binding, but at a later time during the experiment the same PtNP may yield subsequent current pulses. If this is true, can we distinguish between the first hybridization event and subsequent interactions between that PtNP label and the electrode? Do all hybridization events result in current transients, or are there specific molecular environments that are more prone than others to yield an electrochemical signature of hybridization? Is it possible to use the concepts described here to build useful biosensors? How sensitive is this method to single-base mismatches? Will the principles reported here translate to other types of detection motifs, such as DNA and antibody sandwich assays? These are all questions we hope to be able to answer in forthcoming publications.

Acknowledgements

We gratefully acknowledge financial support from the U.S. Defense Threat Reduction Agency (Grant No. HDTRA1-11-1-0005). E. G. N. acknowledges graduate fellowship support from the Department of Defense (DoD) through the Air Force Office of Scientific Research, National Defense Science and Engineering Graduate Fellowship (NDSEG) program 32 CFR 168a. We are indebted to Prof. Allen J. Bard, Prof. Keith J. Stevenson (UT Austin) and Prof. Bo Zhang (University of Washington) for helpful discussions. We also thank Dwight Romanovicz (ICMB, UT Austin), Jim Loussaert (Crooks group, UT Austin), and Hugo Celio (TMI/CNM, UT Austin) for assistance with the TEM and XPS measurements, respectively. We also thank Morgan Anderson (Crooks group, UT-Austin) for carrying out the Comsol Multiphysics 4.3 simulations.

References

1 N. V. Rees, Y.-G. Zhou and R. G. Compton, *RSC Adv.*, 2012, **2**, 379–384.
2 Y. C. Cao, R. Jin and C. A. Mirkin, *Science*, 2002, **297**, 1536–1540.
3 T. A. Taton, C. A. Mirkin and R. L. Letsinger, *Science*, 2000, **289**, 1757–1760.
4 R. Polsky, R. Gill, L. Kaganovsky and I. Willner, *Anal. Chem.*, 2006, **78**, 2268–2271.
5 R. Gill, R. Polsky and I. Willner, *Small*, 2006, **2**, 1037–1041.
6 K.-F. Chow, F. Marvé and R. M. Crooks, *J. Am. Chem. Soc.*, 2008, **130**, 7544–7545.
7 F. Marvé, R. K. Anand, D. R. Laws, K.-F. Chow, B.-Y. Chang, J. A. Crooks and R. M. Crooks, *Anal. Chem.*, 2010, **82**, 8766–8774.
8 S. J. Kwon and A. J. Bard, *J. Am. Chem. Soc.*, 2012, **134**, 10777–10779.
9 A. J. Bard, H. Zhou and S. J. Kwon, *Isr. J. Chem.*, 2010, **50**, 267–276.
10 X. Xiao and A. J. Bard, *J. Am. Chem. Soc.*, 2007, **129**, 9610–9612.
11 S. J. Kwon and A. J. Bard, *J. Am. Chem. Soc.*, 2012, **134**, 7102–7108.
12 Y.-G. Zhou, N. V. Rees and R. G. Compton, *Angew. Chem., Int. Ed.*, 2011, **50**, 4219–4221.
13 Y.-G. Zhou, N. V. Rees, J. Pillay, R. Tshikhudo, S. Vilakazi and R. G. Compton, *Chem. Commun.*, 2012, **48**, 224–226.
14 Y.-G. Zhou, N. V. Rees and R. G. Compton, *Chem. Commun.*, 2012, **48**, 2510–2512.
15 N. V. Rees, Y.-G. Zhou and R. G. Compton, *ChemPhysChem*, 2011, **12**, 1645–1647.
16 Y.-G. Zhou, N. V. Rees and R. G. Compton, *ChemPhysChem*, 2011, **12**, 2085–2087.
17 I. J. Cutress, N. V. Rees, Y.-G. Zhou and R. G. Compton, *Chem. Phys. Lett.*, 2011, **514**, 58–61.
18 Y.-G. Zhou, N. V. Rees and R. G. Compton, *Chem. Phys. Lett.*, 2011, **511**, 183–186.
19 S. Sorgenfrei, C.-y. Chiu, R. L. Gonzalez, Y.-J. Yu, P. Kim, C. Nuckolls and K. L. Shepard, *Nat. Nanotechnol.*, 2011, **6**, 126–132.
20 M. Singh-Zocchi, S. Dixit, V. Ivanov and G. Zocchi, *Proc. Natl. Acad. Sci. U. S. A.*, 2003, **100**, 7605–7610.
21 F. Ricci, A. J. Bonham, A. C. Mason, N. O. Reich and K. W. Plaxco, *Anal. Chem.*, 2009, **81**, 1608–1614.
22 A. A. Lubin and K. W. Plaxco, *Acc. Chem. Res.*, 2010, **43**, 496–505.
23 A. B. Steel, T. M. Herne and M. J. Tarlov, *Anal. Chem.*, 1998, **70**, 4670–4677.
24 Y. Xia and G. M. Whitesides, *Angew. Chem., Int. Ed.*, 1998, **37**, 550–575.
25 A. J. Bard and L. R. Faulkner, *Electrochemical Methods: Fundamentals and Applications*, Wiley, New York, 2000.
26 B. Zhang, M. Wood and H. Lee, *Anal. Chem.*, 2009, **81**, 5541–5548.
27 Y. Li, J. T. Cox and B. Zhang, *J. Am. Chem. Soc.*, 2010, **132**, 3047–3054.
28 J. C. Hoogvliet, M. Dijksma, B. Kamp and W. P. van Bennekom, *Anal. Chem.*, 2000, **72**, 2016–2021.
29 K. I. Ozoemena and T. Nyokong, *Talanta*, 2005, **67**, 162–168.
30 U. Rant, K. Arinaga, S. Fujita, N. Yokoyama, G. Abstreiter and M. Tornow, *Nano Lett.*, 2004, **4**, 2441–2445.
31 U. Rant, K. Arinaga, S. Fujita, N. Yokoyama, G. Abstreiter and M. Tornow, *Org. Biomol. Chem.*, 2006, **4**, 3448–3455.
32 E. A. Josephs and T. Ye, *J. Am. Chem. Soc.*, 2012, **134**, 10021–10030.
33 X. Xiao, F.-R. F. Fan, J. Zhou and A. J. Bard, *J. Am. Chem. Soc.*, 2008, **130**, 16669–16677.
34 D. L. Nelson and M. M. Cox, *Lehninger Principles of Biochemistry*, 5th edn, Freeman, New York, 2008.
35 R. G. Sosnowski, E. Tu, W. F. Butler, J. P. O'Connell and M. J. Heller, *Proc. Natl. Acad. Sci. U. S. A.*, 1997, **94**, 1119–1123.
36 E. Paleček and F. Jelen, in *Electrochemistry of Nucleic Acids and Proteins: Towards Electrochemical Sensors for Genomics and Proteomics*, ed. E. Paleček, F. Scheller and J. Wang, Elsevier, Amsterdam, The Netherlands, 2005, vol. 1, pp. 74-173.

